JOURNAL OF MATERIALS SCIENCE 15 (1980) 469–476

Energy-dispersive X-ray diffraction studies of the texture in cold-rolled alpha-beta brass*

J. SZPUNAR
Department of Metallurgy, Risø National Laboratory, DK-4000 Roskilde, Denmark†

L. GERWARD
Laboratory of Applied Physics III, Technical University of Denmark, DK-2800 Lyngby, Denmark

It is shown that energy-dispersive X-ray diffraction can be used for simultaneous measurement of several pole figures and that the accuracy is sufficient for the determination of the crystallite orientation distribution. The method is applied to the study of the texture in Cu–43 wt % Zn duplex alpha–beta brass rolled to 80% reduction.

1. Introduction

Energy-dispersive X-ray diffractometry has some unique advantages compared with the standard angle-dispersive method, but requires some changes in the procedures generally used. The applicability of energy-dispersive diffractometry to texture studies was suggested by Szpunar [1] and later experimentally demonstrated by Laine and Lähteenmäki [2]. Szpunar *et al.* [3] and Gerward *et al.* [4] showed that energy-dispersive diffraction can be used for the determination of inverse pole figures.

The analysis of preferred orientation has now gone beyond pole figures, in the direction of a more complete description of the texture using the crystallite orientation distribution, called ODF. This function can be calculated from a number of pole figures of one and the same specimen. Energy-dispersive diffraction should be a promising method for ODF studies, one of the advantages being that all the necessary pole figures can be determined in a single experimental run.

The purpose of the present work is to show the advantages of the energy-dispersive method by investigating the rolling texture of Cu–43 wt % Zn duplex alpha–beta brass rolled to 80% reduction.

2. Comparison between the angle-dispersive and energy-dispersive methods for texture analysis

Standard angle-dispersive methods for texture analysis make use of monochromatic X-rays. To determine an $(h\,k\,l)$ pole figure the counter has to be fixed at the proper 2θ angle to receive the $h\,k\,l$ reflection. Between two subsequent intensity measurements the specimen is rotated in a particular way. The direction of the diffraction vector in each measurement is described by the angles α and β, where α is the angle between the normal to the rolling plane and the diffraction vector, and β the angle between the rolling direction and the projection of the diffraction vector on the rolling plane (Fig. 1). The α–β scan has to be repeated for each pole figure that one wants to determine. The absorption correction that one has to apply depends on the variables α and θ. The resolution is best for large Bragg angles, i.e. in the range of back-scattering.

The energy-dispersive method is based on the use of a "white" incident beam. The detector can then be set at any convenient scattering angle and all Bragg reflections are recorded simultaneously at the same Bragg angle, which is called

* Some preliminary results of this work were presented at the Fifth International Conference on Texture of Materials, RWTH Aachen, March 29–31, 1978.

† On leave from Institute of Physics and Nuclear Techniques, University of Mining and Metallurgy, Cracow, Poland. Now returned.

0022–2461/80/020469–8$02.80/0

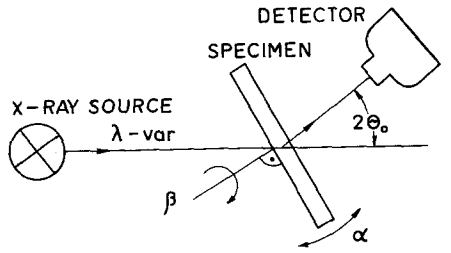

Figure 1 Transmission method for pole-figure determination using energy-dispersive X-ray diffraction. $2\theta_0$ fixed scattering angle; α rotation about the diffractometer axis; β rotation about an axis perpendicular to the specimen surface.

θ_0 in the following (Fig. 1). Pole figures are obtained by stepwise scanning over α and β. In each point (α, β) a diffraction spectrum is recorded (cf. Fig. 3) and the integrated intensities of the wanted Bragg reflections are calculated. Several pole figures are recorded simultaneously, which means a time saving as compared with the standard angle-dispersive method. In addition, the energy-dispersive method makes it possible to separate the intensities of overlapping diffraction peaks, which is very difficult in angle-dispersive texture measurements.

A complication in the energy-dispersive method is the strong wavelength dependence of the absorption correction [4]. Analytic approximations for the X-ray linear absorption coefficient as a function of wavelength (or energy) have to be used. Another consequence of the varying absorption coefficient is that the penetration depth depends on the wavelength. As in the conventional method the penetration depth will also depend on the geometry during the sample rotation (α and θ_0 in the present work).

The optimum resolution of the energy-dispersive method has been discussed by Buras *et al.* [5]. For the angular divergence $\Delta\theta_0 \geqslant 0.3^\circ$, which is commonly used in X-ray work, the resolution is best for large Bragg angles as it is in standard diffraction methods. However, using a very small divergence $\Delta\theta_0 \leqslant 0.01^\circ$, one finds an optimum resolution in the low-angle range where θ_0 equals a few degrees. Such a small divergence may be achieved using a high-intensity X-ray source, e.g. synchrotron radiation.

The energy-dispersive method is well suited for *in situ* studies on samples subjected to various controlled environments. This was shown by Gerward *et al.* [4] in a dynamic tension experiment on an aluminium wire. Another interesting experiment would be to follow a recrystallization texture as a function of temperature by heating a sample.

3. Experimental procedure

The samples are Cu–43% Zn brass consisting of the alpha (b c c) and beta (f c c) phases. The material was rolled to achieve 80% reduction. A metallographic observation (Fig. 2) shows a marked grain elongation for both phases. The samples were cut and polished to a thickness of 0.04 mm for the transmission studies and 1.5 mm for the reflection studies.

Fig. 1 shows the diffraction arrangement in transmission. The continuous X-ray spectrum from a copper tube was used. The diffracted X-rays were energy analysed using a Si(Li) detector. A more detailed description of the equipment has been given elsewhere [6].

Fig. 3 shows a diffraction spectrum of an annealed sample. Some peaks are overlapping but the 0 0 2, 0 2 2 and 1 1 3 reflections from the alpha phase and the 0 0 2, 1 1 2 and 1 2 3 reflections from the beta phase are well resolved so that the integrated intensities can be measured. These reflections have been used for the simultaneous measurement of the corresponding pole figures. The values of α and β were changed in 10° steps.

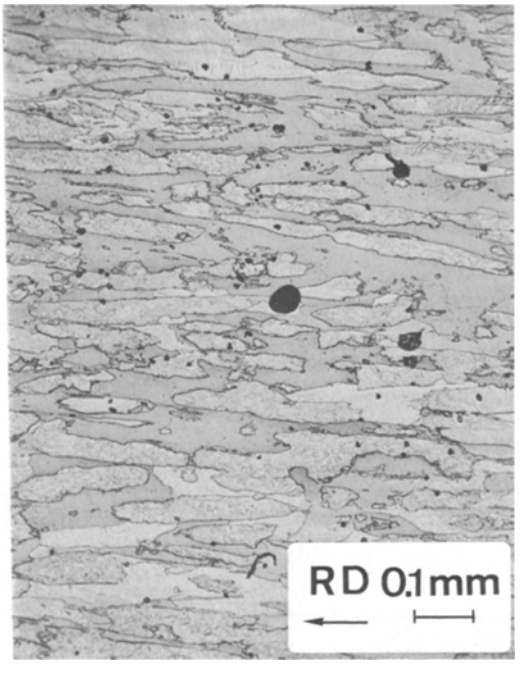

Figure 2 Photograph of the microstructure in Cu–43 wt% Zn after rolling.

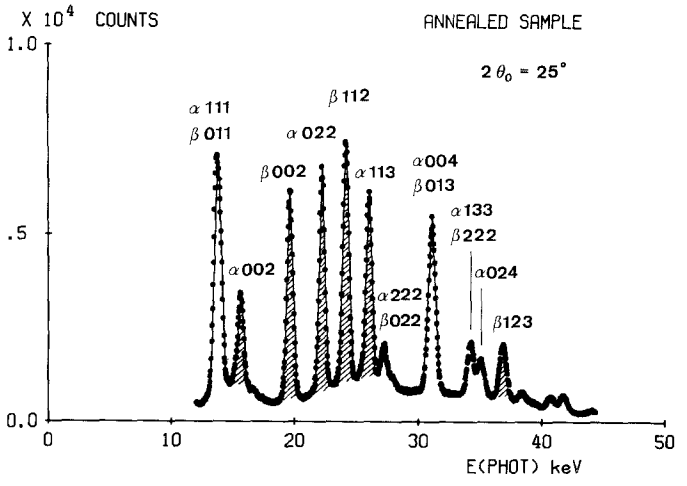

Figure 3 Energy-dispersive diffraction spectrum of an annealed Cu–43 wt % Zn sample.

At each step a diffraction spectrum was recorded for 1000 sec.

The wavelength dependence of the linear absorption coefficient, μ, was found by fitting the absorption data for Cu and Zn given in the "International Tables for X-ray Crystallography", Vol. IV [7] to a Victoreen's approximation:

$$\mu/\rho = C\lambda^3 - D\lambda^4 \qquad (1)$$

where ρ is the density of mass and C and D are fitting parameters. The absorption corrections were then calculated according to the well-known formulae for the transmission method and the Schultz reflection method [8]. Table I shows that the absorption correction for the transmission method changes considerably within the measured angle range. For the reflection case there was no significant change of the absorption factor. Thus the reflection measurements were not corrected for absorption.

4. Results

Figs. 4 and 5 show on their left-hand side the measured pole figures for the alpha phase and the beta phase, respectively. From these pole figures three-dimensional orientation distribution functions (ODF) were calculated following the method described by Bunge [9].

The orientation distribution function, $f(\phi_1, \phi, \phi_2)$, describes the volume fraction, dV/V, of crystallites oriented in a small angular range around the Euler angles, ϕ_1, ϕ and ϕ_2:

$$dV/V = (1/8\pi^2) f(\phi_1, \phi, \phi_2) \sin\phi \, d\phi_1 \, d\phi \, d\phi_2 \qquad (2)$$

The function has the following mathematical form:

$$f(\phi_1, \phi, \phi_2) = \sum_{l=0}^{\infty} \sum_{\mu=1}^{M(l)} \sum_{\nu=1}^{N(l)} C_l^{\mu\nu} T_l^{\mu\nu}(\phi_1, \phi, \phi_2) \qquad (3)$$

where $C_l^{\mu\nu}$ are expansion coefficients and $T_l^{\mu\nu}(\phi_1, \phi, \phi_2)$ are generalized spherical harmonics, invariant with respect to the crystal symmetry and the statistical symmetry of the specimen. The sharpness, I, of the texture is defined as

$$I = (I_1 - 1)/(I_1 + 1)$$

where

$$I_1 = \sum_{l=0}^{\infty} \sum_{\mu=1}^{M(l)} \sum_{\nu=1}^{N(l)} (C_l^{\mu\nu})^2/(2l+1) \qquad (4)$$

Figs. 6 and 7 show the orientation distribution

TABLE I Absorption corrections for the transmission method. Sample thickness 0.04 mm

α	E = 15.7 keV Alpha 0 0 2	E = 19.6 keV Beta 0 0 2	E = 22.3 keV Alpha 0 2 2	E = 24.1 keV Beta 1 1 2	E = 26.1 keV Alpha 1 1 3	E = 37.1 keV Beta 1 2 3
90°	1.000	1.000	1.000	1.000	1.000	1.000
80°	0.986	0.968	0.962	0.959	0.956	0.950
70°	1.027	0.950	0.924	0.912	0.902	0.878
60°	1.149	0.953	0.890	0.861	0.840	0.786
50°	1.431	0.993	0.867	0.813	0.772	0.675
40°	2.149	1.124	0.877	0.779	0.707	0.550

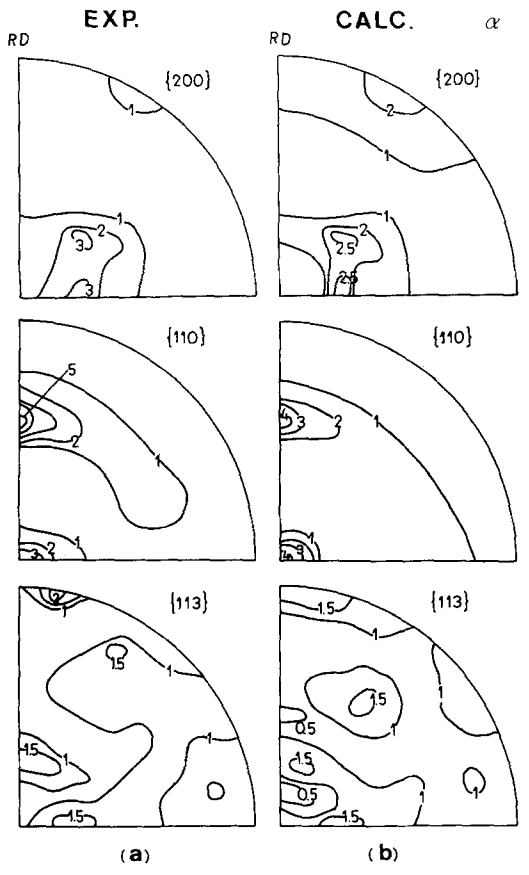

Figure 4 Pole figures of the alpha phase in Cu–43 wt % Zn. (a) Experimental; (b) calculated from the ODF expansion coefficients.

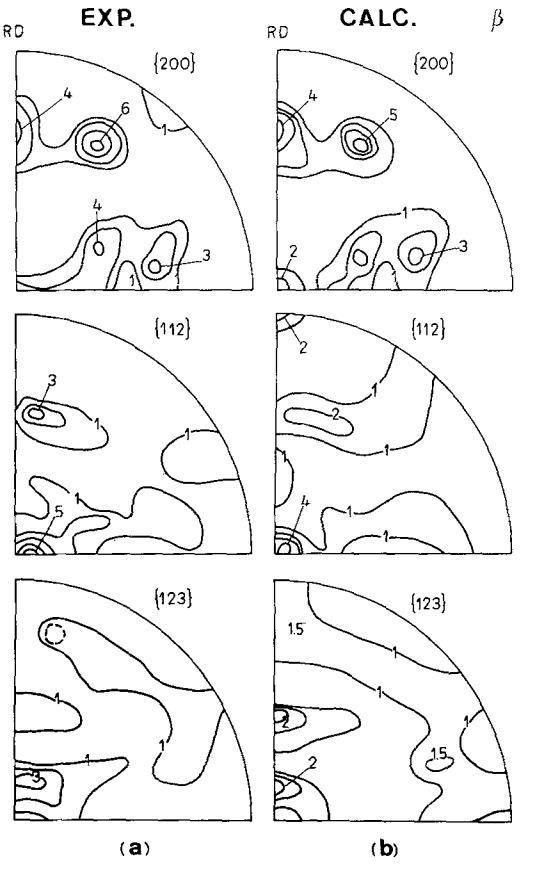

Figure 5 Pole figures of the beta phase in Cu–43 wt % Zn. (a) Experimental; (b) calculated from the ODF expansion coefficients.

functions in ϕ_1-sections for the alpha phase and the beta phase respectively. The texture is found to be stronger in the beta brass than in the alpha brass. Equation 4 gives $I = 0.8$ for the beta brass and $I = 0.3$ for the alpha brass.

5. Discussion

Texture can be often described by the traditional concept of ideal orientations. However, because of the rather complicated texture of both phases in the specimen investigated it is helpful to make use of the texture skeleton line. The projection of the skeleton line in the reference frame of the crystal is shown in Fig. 8 for the case of the alpha brass. The lines denoted by A and B in the right-hand part of the figure represent the orientation of the rolling direction. The corresponding lines a and b in the left-hand part of the figure represent the orientation of the direction normal to the rolling plane.

One notices that the line a is very close to the $(0\,\bar{1}\,1)$ pole so that the texture described by the lines a and A can be expressed in terms of ideal orientations $(0\,\bar{1}\,1)$ $[u\,v\,w]$. The component $(0\,\bar{1}\,1)$ $[\bar{2}\,1\,1]$ has been found to be the strongest one, the pole density being about two times higher than for the $(0\,\bar{1}\,1)$ $[\bar{1}\,1\,1]$ or the $(0\,\bar{1}\,1)$ $[\bar{7}\,1\,1]$ orientations. This is illustrated in Fig. 9 showing the ODF values along the skeleton line. Apart from the orientations already mentioned there are other ideal orientations, for example $(\bar{1}\,\bar{1}\,2)$ $[1\,1\,1]$. Also the texture $(0\,0\,1)$ $[0\,1\,0]$ has been found in the alpha brass.

The texture of the beta brass is rather difficult to describe using ideal orientations. The lines a and A in Fig. 10 shows the strongest texture system. The normal direction lies on the line indicated by a from the $(\bar{1}\,\bar{1}\,1)$ pole through $(\bar{5}\,\bar{3}\,3)$ to $(\bar{3}\,\bar{1}\,1)$ and $(\bar{5}\,\bar{1}\,1)$. The rolling direction lies on the line A from $[1\,1\,2]$ through $[1\,3\,5]$ to $[0\,1\,1]$. The ODF value is lowest for the $(\bar{1}\,\bar{1}\,1)$ $[1\,1\,2]$ orientation and increases as the rolling

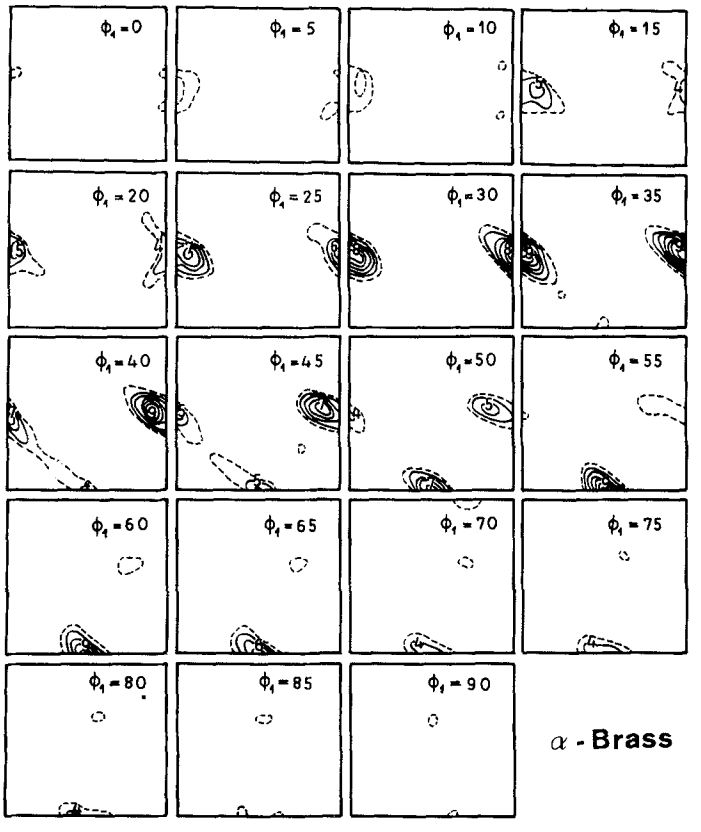

Figure 6 Orientation distribution function (ODF) for the alpha phase in Cu–43 wt % Zn.

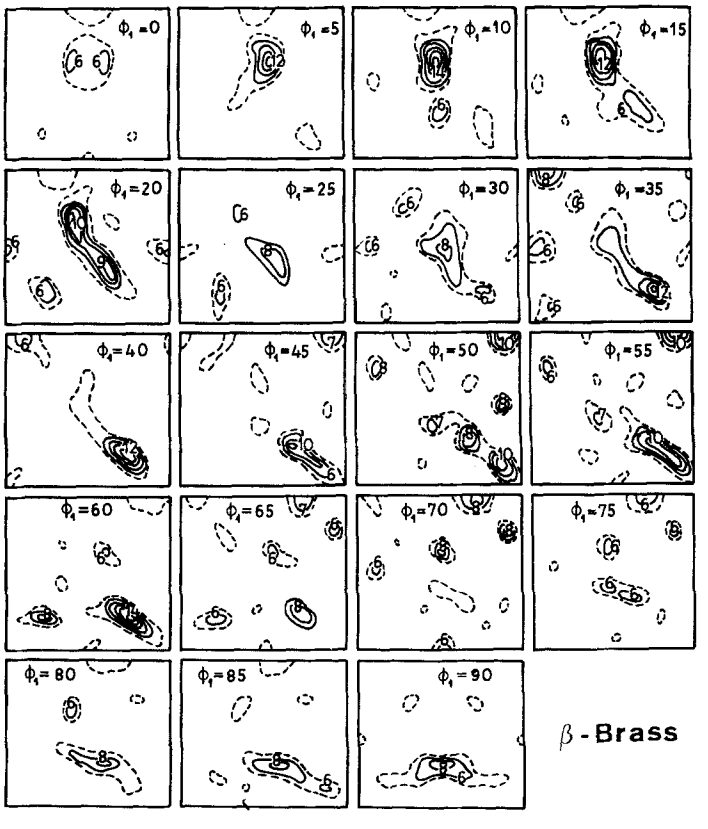

Figure 7 Orientation distribution function (ODF) for the beta phase in Cu–43 wt % Zn.

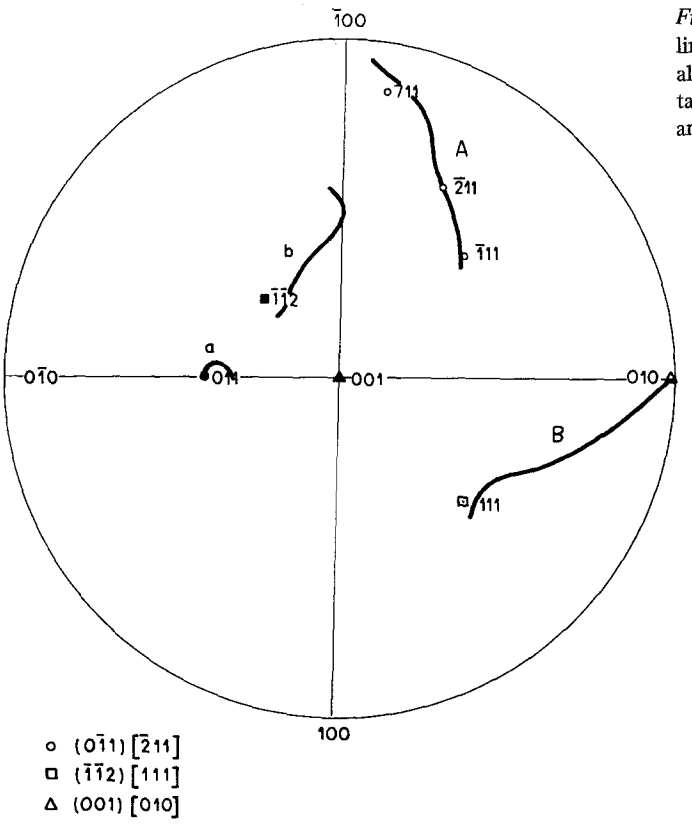

Figure 8 Projection of the texture skeleton lines in the crystal reference frame for the alpha phase. *a* and *b* represent the orientation of the normal to the rolling plane, and *A* and *B* the rolling direction.

direction is changed towards [1 3 5] and [0 1 1]. In addition, texture orientations such as (0 0 1) [$\bar{1}$ 1 0] and ($\bar{1}$ 0 1) [1 1 1] are observed as indicated by the skeleton lines *b*, *B*, *c* and *C* in Fig. 10.

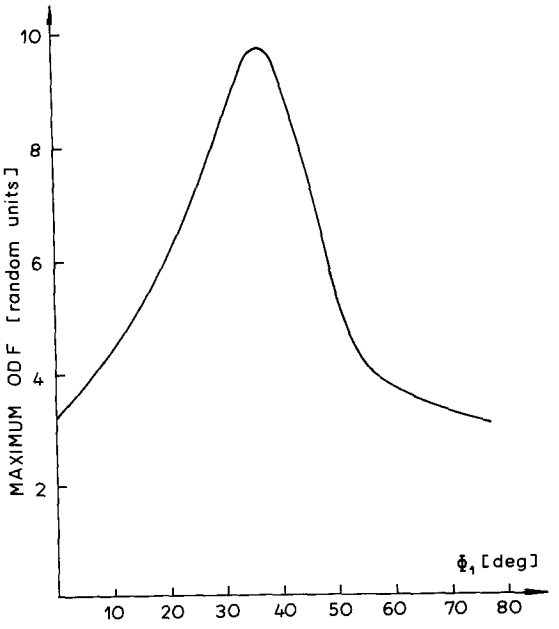

Figure 9 ODF values along the skeleton line *A* for the alpha phase.

The last-mentioned textures are very diffuse, however.

The accuracy in the texture analysis depends mainly on the counting statistics of the recorded X-ray intensities, the number of points in the α–β scan, the accuracy of the ODF expansion (truncation error) and the accuracy of the absorption corrections.

In order to estimate the accuracy of the analysis we have calculated the mean absolute values, C_l, of the ODF coefficients and the standard errors, $\sigma(C_l)$, of these coefficients. The following definitions have been used

$$C_l = \frac{1}{M(l)N(l)} \sum_{\mu=1}^{M(l)} \sum_{\nu=1}^{N(l)} |C_l^{\mu\nu}|$$
$$\sigma(C_l) = \frac{1}{M(l)N(l)} \sum_{\mu=1}^{M(l)} \sum_{\nu=1}^{N(l)} \sigma(C_l^{\mu\nu}) \quad (5)$$

The mean absolute values of the ODF coefficients are compared with their standard errors in Fig. 11.

Another way of estimating the accuracy of the texture analysis is to compare the experimental pole figures with those calculated from the ODF expansion coefficients. This comparison has been done in Figs. 4 and 5, and it can be seen that the

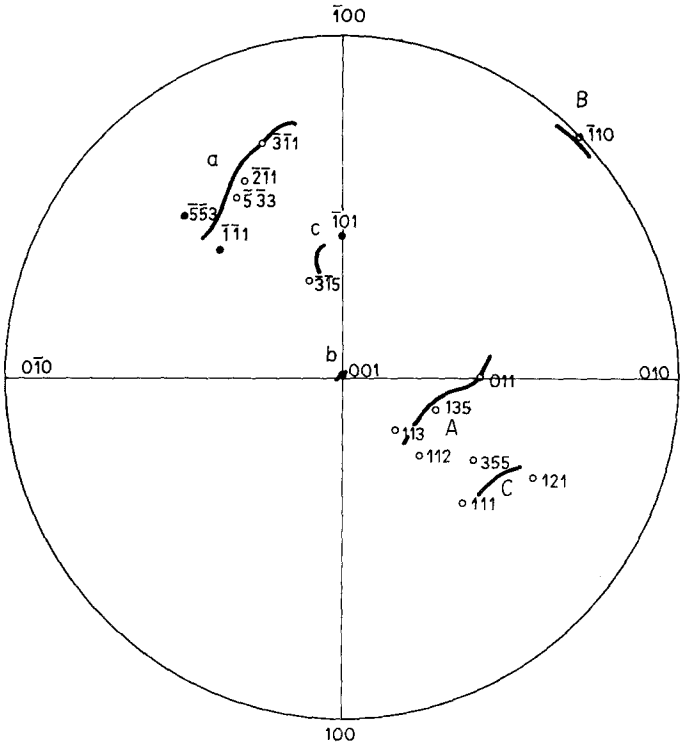

Figure 10 Projection of the texture skeleton lines for the beta phase. Same notation as in Fig. 8.

agreement is good. However, one should be aware that the calculated pole figures should not be considered as the true pole figures. They are more accurate than each of the experimental pole figures because they have been calculated from the ODF expansion coefficients, and these coefficients have been calculated using all the available experimental information from three pole figures.

6. Conclusions

We have shown that the energy-dispersive X-ray diffraction method can be used for the simultaneous measurement of several pole figures, and that the accuracy of the method is sufficient for the determination of the orientation distribution function, ODF.

The method has been applied to the determi-

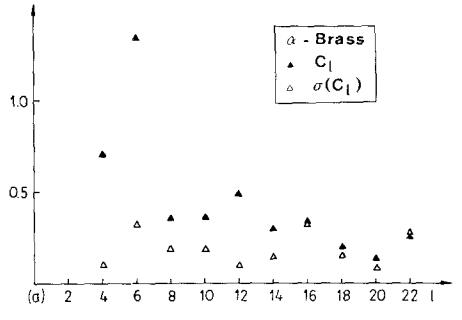

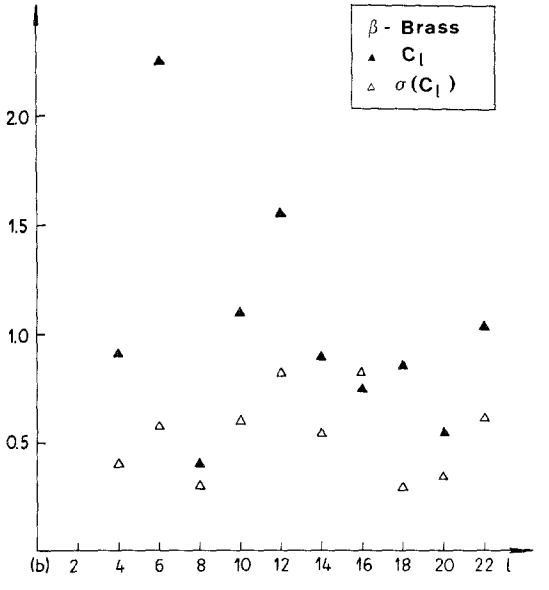

Figure 11 Averaged ODF expansion coefficients (filled symbols) and the corresponding standard errors (open symbols). (a) Alpha phase; (b) beta phase.

nation of texture in duplex alpha–beta brass rolled to 80% reduction. The alpha phase shows a texture that can be expressed in terms of a $(0\,\bar{1}\,1)\ [\bar{2}\,1\,1]$ component. However, there are also other orientations present. The texture in the beta phase is stronger than in the alpha phase. Its complicated texture is difficult to describe using ideal orientations.

Acknowledgements

The authors wish to thank Dr T. Leffers for valuable discussions.

References

1. J. SZPUNAR, *Hutnik* **1** (1968) 49.
2. E. LAINE and I. LÄHTEENMÄKI, *J. Mater. Sci.* **6** (1971) 1418.
3. J. SZPUNAR, M. OJANEN and E. LAINE, *Z. Metallkde.* **65** (1974) 221.
4. L. GERWARD, S. LEHN and G. CHRISTIANSEN, *Texture* **2** (1976) 95.
5. B. BURAS, N. NIIMURA and J. STAUN OLSEN, *J. Appl. Cryst.* **11** (1978) 137.
6. B. BURAS, J. STAUN OLSEN, L. GERWARD, B. SELSMARK and A. LINDEGAARD-ANDERSEN, *Acta Cryst.* **A31** (1975) 327.
7. "International Tables for X-ray Crystallography", Vol. IV (Kynoch Press, Birmingham, 1974).
8. G. WASSERMAN and J. GREWEN, "Texturen metallischer Werkstoffe", 2nd edn (Springer Verlag, Berlin, 1962).
9. H. J. BUNGE, "Mathematischer Methoden der Texturanalyse" (Akademie-Verlag, Berlin, 1969).

Received 26 June and accepted 19 July 1979.